Nickel contamination on MWCNT is related to particle bioactivity but not toxicity in the THP-1 transformed macrophage model

Raymond F. Hamilton Jr. and Teri A. Girtsman

Center for Environmental Health Sciences,
University of Montana,
Missoula MT, 59812, USA
E-mail: ray.hamilton@mso.umt.edu
E-mail: teri.girtsman@mso.umt.edu

Chengcheng Xiang and Nianqiang Wu

Department of Mechanical and Aerospace Engineering,
WV Nano Initiative, West Virginia University,
Morgantown, WV 26506-6106, USA
E-mail: cxiang@mix.wvu.edu
E-mail: Nick.Wu@mail.wvu.edu

Andrij Holian*

Center for Environmental Health Sciences,
University of Montana,
Missoula MT, 59812, USA
Fax: +1 (406) 243-2807
E-mail: andrij.holian@mso.umt.edu
*Corresponding author

Abstract: The potential pathogenic effects from exposure to various MWCNT have not been adequately determined. One potential contributing factor to MWCNT bioactivity could be metal contamination that occurs during production. This study examined the toxicity and bioactivity (NLRP3 inflammasome activation), of 24 commercially available MWCNT in a macrophage-like differentiated THP-1 cell line. Inflammasome activation, via IL-1β release, was highly correlated to Ni content. Soluble $NiCl_2$ and insoluble Ni nanopowder were tested in the same model at varying concentrations with no inflammasome activation. Ni-decorated MWCNT were also tested in the THP-1 model and the results also correlated with Ni content. These results demonstrated that Ni content correlated to NLRP3 inflammasome activation, but not toxicity. Taken together, the results suggest that Ni, when fixed to MWCNT, is highly bioactive and potentially proinflammatory. The related mechanism probably involves lysosomal rupture, release of cathepsin B, and NLRP3 activation.

Keywords: nickel; multi-walled carbon nanotubes; MWCNT; NLRP3 inflammasome; macrophage.

Reference to this paper should be made as follows: Hamilton Jr., R.F., Girtsman, T.A., Xiang, C., Wu, N. and Holian, A. (2013) 'Nickel contamination on MWCNT is related to particle bioactivity but not toxicity in the THP-1 transformed macrophage model', *Int. J. Biomedical Nanoscience and Nanotechnology*, Vol. 3, Nos. 1/2, pp.107–126.

Biographical notes: Raymond F. Hamilton Jr. studied music at San Jacinto Jr. College (Pasadena TX). He also studied statistics and neuroscience at the University of Houston (Clear Lake City, TX) and received a graduate degree. He worked as a Statistician for the University of Texas Graduate School of Biomedical Sciences (1986–1989); and as a Research Associate for the University of Texas Medical School (1989–2000); and as a Researcher/Statistician for the Center of Environmental Health Sciences at the University of Montana from 2000 to present. The present focus of his work is the effects of inhaled particles especially engineered nanomaterials.

Teri A. Girtsman received her BS (2002) and MS (2004) in Cell and Molecular Biology from San Francisco State University (San Francisco, CA). She earned her PhD in Toxicology (2009) from The University of Montana. Currently, she works as an NRSA Postdoctoral Fellow for the Center for Environmental Health Sciences at The University of Montana (Missoula, MT). Her studies focus on uptake mechanisms of ENM and NLRP3 inflammasome activation.

Chengcheng Xiang received her Master in Material Physics at Central South University (China) in 2007, and in Industrial Engineering at West Virginia University (WVU) in 2011. She is a PhD student of Operational Research in the Department of Industrial and Management System Engineering, WVU from 2011 to present. She is supervised by Professor Nianqiang Wu. The focus of her study is synthesis and application of nanotubes, graphene, as well as the preparation and properties of electrode materials for supercapacitors.

Nianqiang Wu received his PhD degree from Zhejiang University, China. He is currently an Associate Professor in the Department of Mechanical and Aerospace Engineering at West Virginia University (WVU), USA. His research areas include nanomaterials and nanolithography; chemical sensors and biosensors; photocatalysts and photoelectrochemical cells; and electrochemical devices for energy conversion and storage.

Andrij Holian received his BS in Chemistry from Bowling Green University (OH) and PhD in Chemistry from Montana State University in 1975. He joined the faculty at The University of Pennsylvania after his postdoctoral fellowship training at the same institution. He moved to The University of Texas Houston Health Science Center in 1984 and was also the Director of Research for the Mickey Leland National Urban Air Toxics Research Center. In 2000, he became the Director of the Center for Environmental Health Sciences at the University of Montana. The focus of his study is mechanisms of initiation of inflammation in response to particles.

1 Introduction

Engineered nanomaterials (ENM) possess many unique properties, such as high surface area and tensile strength, which have attracted much interest for technological and biomedical product development (Harris, 1999). ENM such as nickel hydroxide

nanoparticles, nickel oxide treated carbon nanotubes (single and double walled), as well multi-walled carbon nanotubes (MWCNT) fabricated over nickel catalyst, are in high demand for energy conversion and storage devices (Chen et al., 2010; Rocha, 2009; Gao et al., 2008). Specifically, nickel and MWCNT-supported nickel compounds are currently in use in super-capacitor electrodes for hybrid automobiles and solar panels (Gao et al., 2008; Lang et al., 2008; Nam et al., 2008; Lee et al., 2005; Lin et al., 2010).

Human exposure to ENM is inevitable with increasing use. Furthermore, there are concerns that research into the potential health effects is not in stride with the developing nanotechnology (Donaldson and Stone, 2003; Madl and Pinkerton, 2009). Studies evaluating the safety of ENM indicate that significant pathologies can arise following exposure to these materials (Oberdorster, 2010). For example, MWCNT have been shown to provoke allergic, inflammatory and fibrotic pulmonary responses in animal models (Inoue et al., 2009). Also, studies on the toxicity of residues from nickel catalysts used to synthesise MWCNT, reported that these materials were bioavailable to human epithelium (Liu et al., 2007; Cortijo et al., 2010). Moreover, studies assessing the various soluble metals in prosthetic implants reported an association between soluble nickel ions and increased NLRP3 inflammasome activation (Caicedo et al., 2009). Although there is intense interest in describing the mechanisms by which some ENM (including MWCNT) cause inflammation and injury, the underlying mechanism(s) responsible for the toxic properties of ENM remain unclear.

Evaluating the toxicity of ENM provides an important endpoint, however even if a material is not overtly toxic it may nevertheless induce inflammatory effects in human tissues depending on the mechanism of action. Current studies with various known inflammatory particulates and other danger signals indicate that NLRP3 inflammasome activation leading to IL-1β release from macrophages could be a critical determinant in evaluating health risks to nanomaterials (Yazdi et al., 2010; Cassel et al., 2008). Lysosomal rupture and subsequent release of cathepsin B triggersthe multi-protein NLRP3 inflammasome assembly that cleaves pro-caspase-1 into its active form (Tschopp and Schroder, 2010). Activation of NLRP3 inflammasome and IL-1β release are components in what is termed 'sterile' inflammatory responses (Rock et al., 2010). IL-1β is a potent pro-inflammatory cytokine that promotes an array of innate immune processes (Dinarello, 2011a). IL-1β is initially produced as an inactive cytosolic precursor that requires proteolytic cleavage by active caspase-1 for activation and secretion, which occurs following formation of the NLRP3 inflammasome (Dinarello, 2009). Activation of the NLRP3 inflammasome is initiated by a diverse and growing list of endogenous and exogenous agonists (Davis et al., 2011).

In this study, we sought to test the hypothesis that nickel associated with MWCNT can induce bioactivity in differentiated THP-1 cells through activation of the NLRP3 inflammasome activation and subsequent IL-1β release. The ENM evaluated were selected from a collection of commercially available and characterised MWCNT provided to us by the National Toxicology Program (NTP). The nickel content of these MWCNT was from remaining impurities from nickel catalyst bound in the core of the material. The bioactivity of these commercial MWCNT was compared with MWCNT that were fabricated with nickel bound to the surface. The bioactivity of a soluble $NiCl_2$ and a commercial Ni nanopowder were evaluated for comparison purposes. Toxicity and NLRP3 inflammasome induction, assessed by measuring levels of IL-1β protein release, in THP-1 cells exposed to these materials for 24 hours to quantify the bioactivity of MWCNT associated with metal contaminants, particularly Ni.

2 Materials and methods

2.1 Characterisation of MWCNT

Twenty-four MWCNT samples were provided to us by Dr. Nigel Walker and Brad Collins at the NTP at the National Institute of Environmental Health Sciences (NIEHS). Procurement and characterisation of the MWCNT were carried out for the NTP by the Research Triangle Institute under NIEHS contract N01-ES-65554.

Vendor addresses of commercially available MWCNT:

MK Impex	MK Impex Corp, Mississauga, ON, Canada	http://www.mknano.com/
Nano Armor	Nanostructured & Amorphous Materials Inc., Houston, TX	http://www.nanoarmor.com/
Nano Lab	Nano Lab, Inc., Waltham, MA, USA	http://www.nano-lab.com/home.html
Sigma Aldrich	Sigma-Aldrich Corp, St. Louis, MO, USA	http://www.sigmaladrich.com/united-states-html
Sun Innovations	Sun Innovations, Inc., Fremont, CA, USA	http://www.nanomaterialstore.com/
Cheap Tubes	Cheap Tubes.com, Brattleboro, VT, USA	http://cheaptubesinc.com/contact.htm
Helix Material	Helix Material Solutions, Inc., Richardson, TX, USA	http://www.helixmaterial.com/

Purity of each MWCNT was analysed by thermogravimetric analysis. A TA Instruments TGA Q500 ThermogravimetricAnalyzer (TGA) (TA Instruments, New Castle, DE) was used for the analysis. A nominal 10 mg aliquot of each sample was accurately weighed and transferred to a platinum sample pan for analysis. The instrument was gradually ramped to a temperature of 850°C. Duplicate aliquots of each study sample were analysed.

Metal content of each of the MWCNT study samples was determined by X-ray fluorescence (XRF) spectrometry. A nominal 250 mg aliquot of each sample was transferred to an XRF sample cup and sealed with film. Cups were loaded into the ThermoNoranQuant'Xenergy dispersive XRF (Middleton, WI), and were analysed with filter conditions optimised for determination of Fe, Co, Ni, Mo, and Y. Using these filter conditions, the presence of additional metals present at significant levels would also have been detected. Samples were analysed in duplicate fashion.

An FEI Tecnai G^2 Twin (Hillsboro, OR) Transmission Electron Microscope (Shared Materials Instrumentation Facility, Duke University) with an ultrathin carbon type-A, 400 Mesh copper TEM Grid (Ted Pella, Inc., Redding, CA) was used to determine the diameter of the MWCNT samples. Over 50 representative TEM images were taken and an average of > 150 MWCNT was measured for each sample. Fovea Pro software (Reindeer Graphics, Asheville, NC) was used for the diameter measurement. The procedure involved threshold adjustment and MWCNT overlap area masking to obtain accurate measurement of the MWCNT diameters. A comprehensive list of MWCNT characterisation can be found in Table 1.

Table 1 Descriptions and characterisations for 24 commercially available MWCNT

NTP code	*Fe %*	*Co %*	*Ni %*	*Mo %*	*Dia. (nm)*	*Purity %*	*Type*
FA06B	0.401	0.017	1.14	0	28	98.4	Aligned
FA02	0.605	0.005	2.06	0		97.3	Aligned
FA10A	6.43	0	0	2.54	7	91	Aligned
FA20	0.131	0	0.811	0	10	99.1	Long
FA07B	0.0173	0	1.3	0.043	22	98.6	Long
FA33	0.0114	0.012	1.63	0	20	98.4	Long
FA09A	0.0285	0	2.59	0	15	97.4	Long
FA18	0.106	0.74	0.0119	0.391	7	98.8	Long
FA07A	0.168	1.8	0.446	3.46	12	94.1	Long
FA06A	7.16	0	2.64	0	18	90.2	Long
FA03	0.115	4.64	0.0595	7.98	6	87.2	Long
FA09B	5.86	0	0	0	10	94.1	Short
FA08A	0.384	4.07	0.0497	9.11	5	86.4	Short
FA31	0.102	4.51	0.58	13.6	7	81.2	Short
FA19	0.105	4.72	0.61	14.3	7	80.3	Short
FA04	0.0543	0.012	2.54	0.089	33	97.3	Long
FA10B	0.0678	0.018	2.83	0.123	29	97	Long
FA08B	0.0667	0	4.59	0.008	24	95.3	Long
FA17	0.123	0	5.47	0.004	32	94.4	Long
FA21	0.441	0.007	5.54	0.005	27	94	Long
FA13	0.0553	0.010	3.17	0	34	96.8	Short
FA05	0.00971	0.00857	3.65	0.0083	29	96.3	Short
FA22	0.0073	0.01	3.77	0.00685	39	96.3	Short
FA11	0.449	0.00878	5.46	0.0061	45	94.1	Short

2.2 Control nickel (soluble and solid)

Nickel (II) chloride hexahydrate obtained from Sigma/Aldrich (cat # 20,386-6, St Louis, MO) was used as a soluble nickel control. Supplement Figure 1 shows the TEM image of nickel nanoparticles. The particle size was around 7 nm. It was dissolved in ultra-pure water at 50× concentration. Mass was adjusted for the nickel content (22.9%). Therefore, the indicated mass (graphs, text) is for the nickel component only. Nickel nanopowder was obtained from Alfa (cat # 45505, Ward Hill, MA). Stored under argon, the solid Ni core, NiO shell particle was 5–20 nm (7 nm average confirmed) at 99.9% Ni purity. The stock suspension was 1 mg/ml in the 7.5% BSA/DPBS (Sigma, St. Louis, MO) solution used for the MWCNT preparation as described below.

2.3 Nickel-decorated MWCNT preparation and characterisation

MWCNT were purchased from Nanostructured & Amorphous Materials, Inc (Houston, TX). The carboxyl group functionalised MWCNT were prepared by nitric acid oxidation.

Briefly, 300 mg of MWCNT were refluxed at 110°C in 100 ml nitric acid (con. 63%) for 12 hr. The solution was then centrifuged and washed with deionised water to remove excess nitric acid until the pH value was around 6–7. The resulting powders were dried at room temperature in a vacuum oven for at least 24 h. Following this, 100 mg of carboxyl group functionalised MWCNT were added to 5 ml ethanol containing various amounts of $Ni(NO_3)_2$, and ultrasonicated for 1 min, followed by magnetic stirring overnight to adsorb $Ni(NO_3)_2$ onto MWCNT. The solution was then centrifuged to remove excess $Ni(NO_3)_2$, and the black powders were calcined at 300°C for 2 hr in a tubular furnace, which results in the NiO-MWCNT composites. Finally, the as-madeNiO-MWCNT were reduced to Ni-MWCNT through heating at 500°C for 2 hr in a flow of 10% H_2 and 90% N_2 at a rate of 150 sccm. The original mass ratio of Ni (in precursor) to MWCNT was varied at three levels: low (1:25), medium (1:6.25) and high (1:3.125) in order to obtain different loading on MWCNT. The morphology of Ni-decorated MWCNT was observed with scanning electron microscope (SEM) (JEOL, JSM-7600F, Japan). Supplement Figure 2 shows Ni nanoparticle decorated MWCNT with a high level of Ni loading.

2.4 MWCNT suspension preparation

All MWCNT were weighed using a Sartorius analytical balance. The material was placed in a sterile 1.5 ml microfuge tube. All MWCNT were suspended in 7.5% BSA/DPBS solution (cat # A8412, Sigma, St Louis, MO) as described elsewhere (Buford et al., 2007). Nanotube suspensions were sonicated for 1 min in a cup-horn sonicator (Masonix XL2020, Farmingdale, NY) attached to a Forma circulating water-bath at 550 watts and 20 kHz. The final stock suspension was 2 mg/ml. The Ni nanopowder was prepared in the same manner with the exception of the final concentration at 1 mg/ml.

2.5 Cell cultures and MWCNT exposures

THP-1 cells, a human monocytic cell line obtained from ATCC, were suspended in RPMI media (MediaTech, Manassas, VA) supplemented with 10% fetal bovine serum, 50 μM beta-mercapto ethanol, 1 mM sodium pyruvate, 250 ng/ml amphotericin B, and 100 U/ml penicillin and streptomycin (all supplements Media Tech, Manassas, VA) in 75 cm^2 flasks at 37°C. The cells in suspension were differentiated into a macrophage-like cell by adding phorbol 12-myristate 13-acetate (82 nM PMA, sigma) for 24 hr. The adherent cells were washed once with PBS and scrapped with a rubber policeman (Corning, Corning, NY). The cells were then centrifuged at 400 × *g* for 5 min, the resulting cell pellet wasresuspended in 1 ml of complete media, and a 40 μl sample was then counted on a Z2 Coulter Counter (Beckman Coulter, Miami, FL). The cells were suspended at 1×10^6 cells/ml and lipopolysacharride (LPS, Sigma, St Louis, MO) was added at 10 ng/ml. LPS co-stimulation is necessary to induce NF-kB translocation leading to pro-IL-1β synthesis for the NLRP3 inflammasome to cleave for IL-1β release in the transformed THP-1 model (Dostert et al., 2008; Palomaki et al., 2011). Cells, at a volume of 350 μl, were then aliquoted in to 1.5 ml microfuge tubes. The MWCNT or control conditions were added from 2 mg/ml concentrated stock suspensions to the cells at a final concentration of 25 μg/ml. The control Ni and Ni-decorated MWCNT experiments used a range of concentrations (0, 1, 10, 20, and 40 μg/ml). The resulting cell/particle suspension was mixed by pipette action. The cells were then transferred to 96-well tissue culture plates at 100 μl per well in triplicate (100×10^3 cells/well), and

cultured for an additional 24 hr. For the experiments that used the cathepsin B inhibitor (10 μM) Ca-074-Me (Peptides International, Louisville, KY) and caspase-1 inhibitor (20 μM) Ac-Try-Val-Ala CMK (Ana Spec, Fremont, CA), the inhibitors were added 15 min prior to the MWCNT addition described above. All cultures were maintained in 37°C water-jacketed CO_2 incubators (ThermoForma, Houston, TX).

2.6 Assays

2.6.1 LDH membrane integrity assay

CytoTox 96® non-radioactive cytotoxicity assay (Promega, Madison, WI) was used to quantify LDH release at 24 hr post-exposure through conversion of a tetrazolium salt into a red formazan product. To establish a 100% cell death positive control, a lysis solution at 1:10 was added to no particle control cells for 30 min of incubation at 37°C just prior to the end of the 24 hr culture period. At the conclusion of the 24 hr culture, the 96-well plates were centrifuged at 1,000 × *g* for 3 min and 50 μl of media were taken from the cell cultures and placed in fresh 96-well plates to which substrate mix was added (50 μl). Following a 10 min colour-development incubation at RT under light protection, stop solution was added (50 μl), and the absorbance was measured at 490 nm using a microplate reader (Molecular Devices, Sunnyvale CA). Absorption values at 24 hr post-exposure were normalised to lysed 100% kill cells and significance was determined relative to the negative control, where cells exposed to no particles, using one-way ANOVA with Dunnett's test and presented as the mean ± standard error of the mean (*SEM*), with significance indicated at $p < 0.05$ (*), 0.01 (**) or 0.001 (***). Note: This assay does not work well with some MWCNT-exposed cultures due to the fact that the finer particles get trapped in the media, regardless of centrifugation, resulting in a false high optical density or 'false positive' LDH release. Optical density distortions can exceed 0.1 units in some cases. For this reason, the 24 MWCNT conditions were excluded from this assay.

2.6.2 MTS proliferation/cytotoxicity assay

CellTiter 96® AQueous non-radioactive cell proliferation assay (Promega, Madison, WI) was used to quantify cell viability at 24 hr post-exposure through the reduction of MTS (3-(4,5-dimethylthiazol-2-yl)-5-(3-carboxymethoxyphenyl)-2-(4-sulfophenyl)-2H-tetrazolium, inner salt) into aqueous soluble formazan by dehydrogenase enzymes found in metabolically active cells. The MTS solution, in growth media (1:6 dilution), was added to the cells at 120 μl/well (after the media was isolated for LDH and IL-1β assays) for a 1 hr incubation at 37°C. After 1 hr, 100 μl of the MTS/media is mixed with gentle pipette action and transferred to a fresh 96-well plate for the read, to avoid artefacts in optical density caused by cell and particle interference of the light path. Absorbance was measured at 490 nm using a microplate reader (molecular devices). The mean absorbance of no particle control was established as 100% cellular viability. The absorbance of cells exposed to the MWCNT was measured and normalised to no particle control. Significant changes in the normalised values was determined using a one-way ANOVA comparing exposed cells to negative control with Dunnett's test and presented as the mean ± standard error of the mean (*SEM*), with significance indicated at $p < 0.05$ (*), 0.01 (**) or 0.001 (***).

2.6.3 IL-1β assay

Human IL-1β was determined by using DuoSet ELISA from R&D systems (Minneapolis, MN) according to the manufacturer's protocol. Samples were diluted 1:50 or greater to get on to the standard curve. Absorbance was measured at 450 nm using a microplate reader (molecular devices).

2.7 Statistical analyses

Linear regression was used to determine the significant associations between contaminant metals and bioactivity. The coefficient of determination (r^2) describes the strength of association and significance is indicated at a probability of type I error less than 5%. Other analyses included one-way ANOVA followed by Dunnett's test to a single control group to adjust for multi-comparison bias. Two-tailed probability of type I error less than 5% was considered significant. Analyses and graphics were performed with PRISM software (GraphPad, San Diego, CA).

3 Results

3.1 MWCNT nickel contamination is associated with NLRP3 activation in THP-1 cells

The PMA transformed THP-1 cells were exposed to 24 commercially available MWCNT with varying metal contaminations at 25 μg/ml. The principle contaminants were nickel, iron, molybdenum, and cobalt. The cells were co-cultured with a small amount of LPS to stimulate pro-IL-1β production. The degree of activation of NLRP3 by the MWCNT would result in caspase-1 activation and consequently IL-1β release in to the culture media, and the amount of IL-1β would be proportional to the degree of NLPR3 activation. Figure 1 shows the resulting relationship between mean IL-1β release from the THP-1 cells and the MWCNT metal contamination. Figure 1(a) illustrates the highly significant association between THP-1 IL-1β release and the amount of nickel contamination on the MWCNT. In contrast, Figures 1(b), 1(c), and 1(d) indicate that there is no association between IL-1β release and any of the other metal contaminants (Fe, Co, or Mo). The raw data with variance can be found in Supplemental Figure 3(b). Also considered in a linear regression model, but not shown, were the associations between IL-1β release and MWCNT purity, diameter, type, and length. None of these associations was significant (data not shown).

Figure 1 Association between MWCNT metal contamination and *in vitro* measures of MWCNT bioactivity in transformed THP-1 cells, (a) The relationship between nickel contamination and IL-1β production in THP-1 cells (b) The relationship between iron contamination and IL-1β production in THP-1 cells (c) The relationship between cobalt contamination and IL-1β production in THP-1 cells (d) The relationship between molybdenum contamination and IL-1β production in THP-1 cells

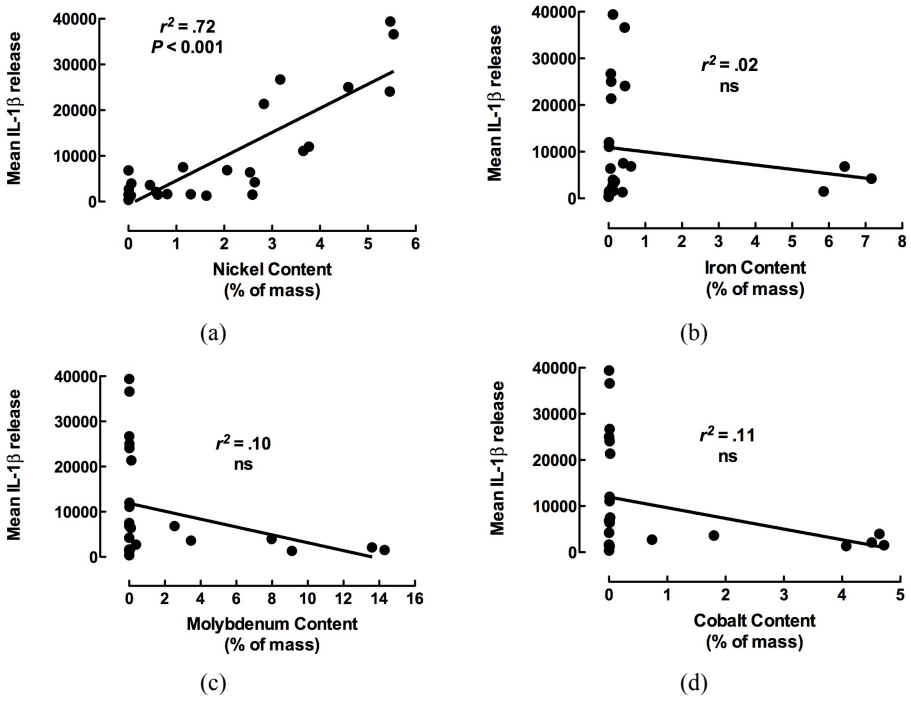

Notes: PMA transformed THP-1 cells (100 µl at 10^6 cells/ml) were incubated with 25 µg/ml of the 24 MWCNT for 24 hr. Release of IL-1β required co-stimulation with 10 ng/ml LPS to generate the pro-form of the cytokine for the NLRP3 inflammasome-activated caspase-1 to process. Asterisks (***) indicate a significant association with $p < 0.001$ resulting from linear regression analysis.

3.2 MWCNT nickel contamination is not associated with toxicity in THP-1 cells

In addition to measuring IL-1β release, cytotoxicity at 24 hr was determined by MTS assay. The relationship between MWCNT cytotoxicity and metal contamination can be found in Figure 2. Nickel and iron show no association with cytotoxicity [Figures 2(a) and 2(b)]. In contrast, cobalt and molybdenum demonstrate a weak, but significant association with THP-1 cytotoxicity [Figures 2(c) and 2(d)]. The raw data with variance can be found in Supplemental Figure 3(a). Taken together with the IL-1β release data it would appear that MWCNT bioactivity and cytotoxicity are independent processes in this model. This is not an artefact of the low concentration. It should be noted that these associations are consistent at other higher concentrations (50 and 100 µg/ml) tried in this model (data not shown).

Figure 2 Association between MWCNT metal contamination and *in vitro* measures of MWCNT toxicity in transformed THP-1 cells, (a) The relationship between nickel contamination and cytotoxicity in THP-1 cells (b) The relationship between iron contamination and cytotoxicity in THP-1 cells (c) The relationship between cobalt contamination and cytotoxicity in THP-1 cells (d) The relationship between molybdenum contamination and cytotoxicity in THP-1 cells

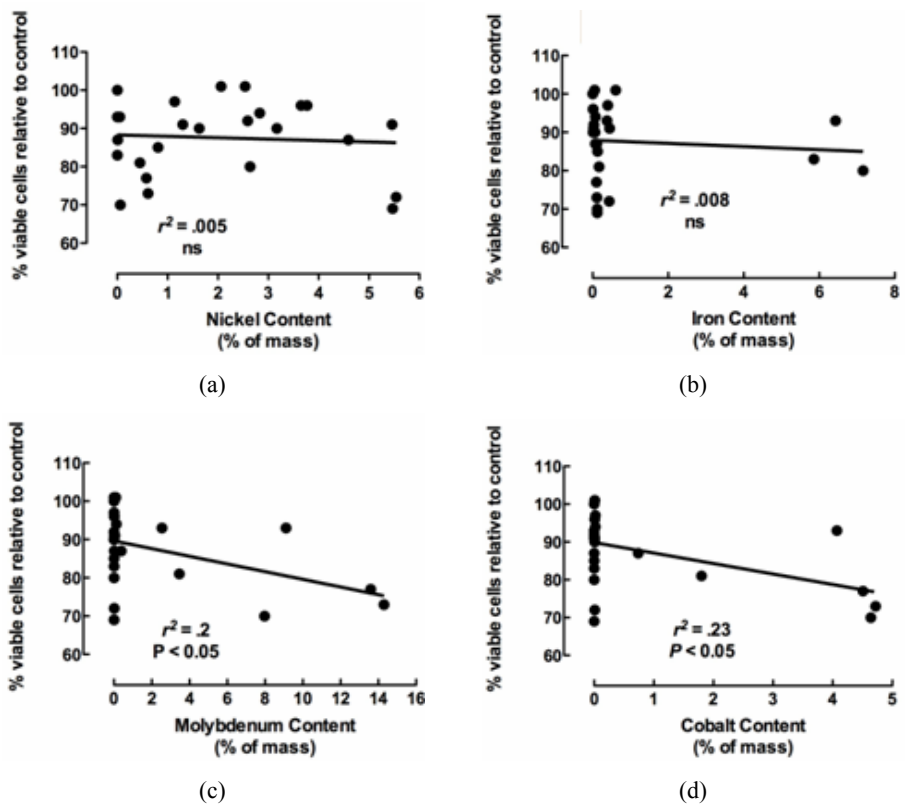

Notes: PMA transformed THP-1 cells (100 µl at 10^6 cells/ml) were incubated with 25 µg/ml of the 24 MWCNT for 24 hr. The resulting toxicity was measured by MTS assay and compared to no particle control condition. Asterisk (*) indicates a mildly significant association with $p < 0.05$ resulting from linear regression analysis.

3.3 Cytotoxicity and bioactivity of soluble and insoluble nickel

Since the nickel contamination had a clear association to IL-1β release, the same THP-1 model was used to determine the possible effect of two types of nickel, soluble and insoluble. The soluble nickel was nickel(II) chloride hexahydrate with the concentration adjusted for the nickel content. The insoluble nickel was a Ni nanopowder with a pure Ni core and a NiO coating. A range of concentrations was tested (1, 10, 20, 40 µg/ml) for both. It is important to note that the 1 µg/ml concentration is the closest to the amount of Ni in the nickel-contaminated MWCNT at 25 µg/ml. Figures 3(a) (LDH) and 3(b) (MTS) show a lack of toxicity with the exception of the highest concentration. Figure 3(c) shows the IL-1β release, which was not significantly different than the model's background

IL-1β release for either Ni form. Taken together, these results indicate that nickel alone, regardless of form, cannot generate NLRP3 activity or cytotoxicity in the THP-1 model.

Figure 3 Soluble nickel and solid nickel nanoparticles do not activate transformed THP-1 cells, (a) Line graph showing the mean ± *SEM* LDH release in response to the Ni stimulants. (b) Line graph showing the mean ± *SEM* percent viable cells in response to the Ni stimulants relative to 0 µg/ml condition (c) Line graph showing the mean ± SEM IL-1β production in response to the Ni stimulants

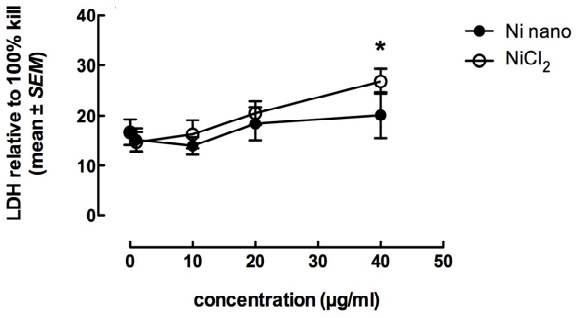

(a)

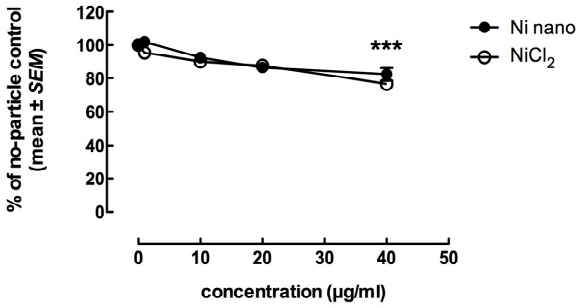

(b)

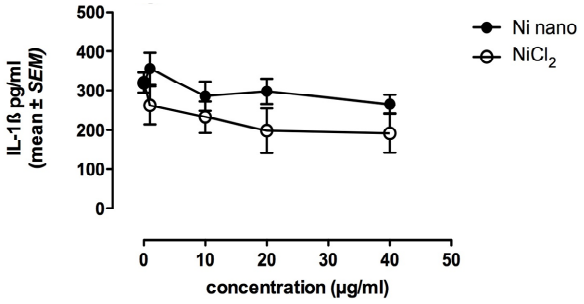

(c)

Notes: PMA transformed THP-1 cells (100 µl at 10^6 cells/ml) were incubated with (0, 1, 10, 20, or 40) µg/ml of either $NiCl_2$ or Ni nanopowder for 24 hr. Cells were co-stimulated with 10 ng/ml LPS to generate the pro-form of the cytokine for the NLRP3 inflammasome-activated caspase-1 to process. Any resulting toxicity was measured by LDH and MTS assays. Asterisk (*) indicates $p < 0.05$, and triple asterisks (***) indicate $p < 0.001$ compared to 0 µg/ml condition.

Figure 4 Nickel-decorated MWCNT mimic NLRP3 activation in transformed THP-1 cells, (a) Line graph showing the mean ± *SEM* LDH release in response to the Ni-decorated MWCNT (b) Line graph showing the mean ± *SEM* percent viable cells in response to the Ni-decorated MWCNT relative to the no particle control condition (c) Line graph showing the mean ± *SEM* IL-1β production in response to the Ni-decorated MWCNT

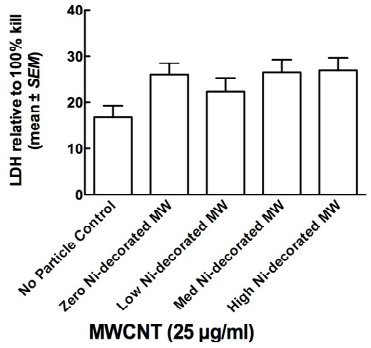

(a)

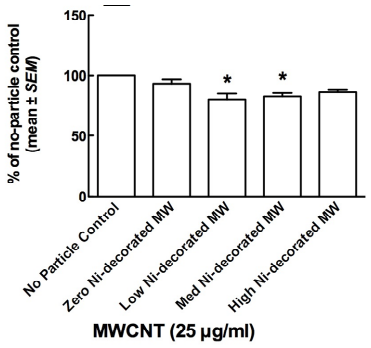

(b)

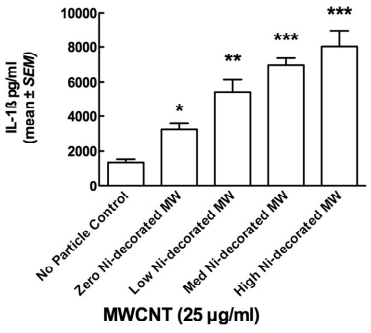

(c)

Notes: PMA transformed THP-1 cells (100 µl at 10^6 cells/ml) were incubated with 25 µg/ml of (0, low, medium and high levels) percent nickel-decorated MWCNT for 24 hr. Cells were co-stimulated with 10 ng/ml LPS to generate the pro-form of the cytokine for the NLRP3 inflammasome-activated caspase-1 to process. Any resulting toxicity was measured by LDH and MTS assays. Asterisk (*) indicates $p < 0.05$, double asterisks (**) indicate $p < 0.01$, and triple asterisks (***) indicate $p < 0.001$ compared to the no particle control condition.

Figure 5 MWCNT-induced NLRP3 inflammasome can be attenuated by cathepsin B and caspase-1 inhibitors, (a) Mean ± *SEM* percent viable cells relative to no particle control cultures (b) Mean ± *SEM* IL-1β release in response to MWCNT exposure

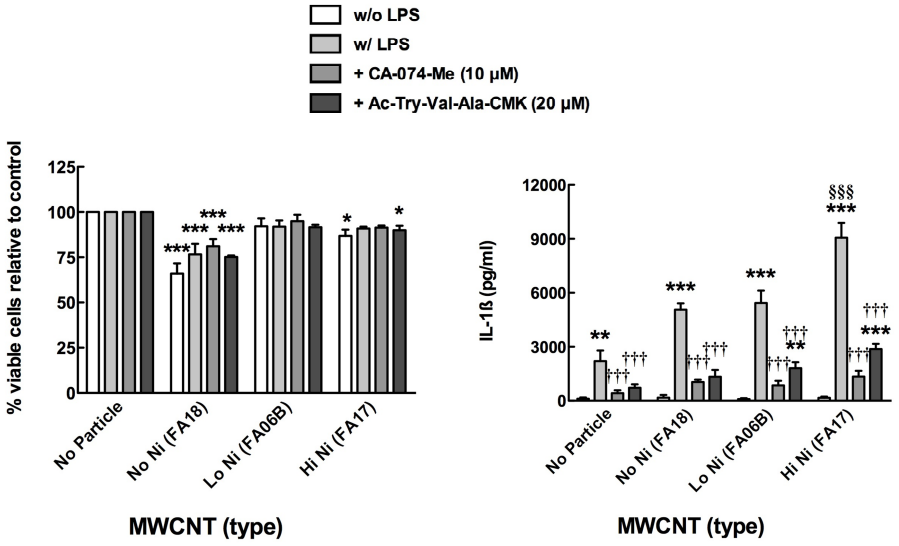

(a) (b)

Notes: PMA transformed THP-1 cells (100 μl at 10^6 cells/ml) were incubated with three (based on Ni content) of the 24 MWCNT for 24 hr. Release of IL-1β required co-stimulation with 10 ng/ml LPS to generate the pro-form of the cytokine for the NLRP3 inflammasome-activated caspase-1 to process. Inhibitors of up-stream NLRP3 inflammasome enzymes cathepsin B (CA-074-Me, 10 μM) and caspase-1 (Ac-Try-Val-Ala-CMK, 20 μM) were pre incubated for 15 min prior to MWCNT exposure. Asterisk (*) indicates $p < 0.05$, double asterisks (**) indicate $p < 0.01$, and triple asterisks (***) indicate $p < 0.001$ compared to corresponding w/o LPS condition. Dagger (†) indicates $p < 0.05$, double daggers (††) indicate $p < 0.01$, and triple daggers (†††) indicate $p < 0.001$ compared to corresponding with LPS condition.§§§ indicates $p < 0.001$ compared to no and low Ni MWCNT. $n = 4$.

3.4 Nickel-decorated MWCNT mimic nickel-contaminated MWCNT

Since nickel alone at equivalent concentrations did not stimulate NLRP3 activation, an artificially nickel-decorated MWCNT was developed and tested in the same THP-1 model. The Ni content was varied as Ni bound to the sidewalls of the MWCNT (0, low, medium, high level). At the same 25 μg/ml dose, the low level of Ni loaded MWCNTs was closest to the nickel-contaminated MWCNT tested earlier. Figure 4(a) (LDH) and 4(b) (MTS) show the relative toxicity of the Ni-decorated MWCNT. Figure 4(a) shows no significant toxicity based on LDH release. This also demonstrates the concern with MWCNT in this assay as the 0% MW was one of the particles that did not centrifuge out, resulting in a false high value (increased OD). The MTS assay shown in Figure 4(b) shows some slight toxicity at the low and medium levels of Ni loading, but not at the high level, which is consistent with the observation that nickel content was not associated with toxicity using THP-1 cells. Figure 4(c) does show a significant dose-dependent increase in IL-1β release. Again, this was entirely consistent with the observation that the Ni

content is associated with the NLRP3 activation in this model. It should be noted however that the absolute IL-1β release is much less than that seen in the contaminated MWCNT. This would indicate that the artificial Ni decoration does not result in exactly the same distribution/accessibility as the Ni distribution that occurs with production of MWNCT.

3.5 MWCNT-induced NLRP3 inflammasome formation can be attenuated by cathepsin B and caspase-1 inhibitors

To demonstrate the role of MWCNT-induced activation of the NLRP3 inflammasome, three of the 21 MWCNT selected based on Ni content (none, low < 2%, or high > 5%) wereincubated with THP-1 cells with selective inhibitors for cathepsin B and caspase-1. In addition, a 'no LPS' condition was added for all MWCNT to demonstrate the necessity of the co-stimulant signal in IL-1β production. The THP-1 cells were cultured for 24 hr with the MWCNT as described above and the MTS assay and IL-1β assay were performed as before. The MTS data shown in Figure 5(a) demonstrated again that Ni content was not related to viability, as the 'no Ni' MWCNT (FA18) was the most toxic. It was also evident that neither inhibitor had an effect on viability. As shown in Figure 5(b), there was a significant reduction of IL-1β in the presence of both cathepsin B and caspase-1 inhibitors with the cathepsin B inhibitor being slightly more effective. The high Ni MWCNT (FA17) exposure was significantly greater than the no or low Ni MWCNT (FA06B) exposure showing again the importance of Ni content in IL-1β production. It is important to note that the no Ni MWCNT (FA18) did produce a significant background IL-1β production indicating that the MWCNT, in the absence of Ni contaminants, can generate some basal NLRP3 inflammasome activation.

4 Discussion

In the field of nanotoxicology a main research focus is to determine the relationships between the properties of nanomaterials and biological activity that would help predict toxicity of new nanomaterials since in vivo testing is impractical to keep pace with development of new materials. Closely associated with this overarching question is to determine which in vitro assays and cell model would be the most predictive of biocompatibility or incompatibility. In order to address this question it is necessary to link the in vitro assay to what is mechanistically understood regarding in vivo pathology. A number of possible variables have been suggested with regard to MWCNT toxicity and bioactivity including particle shape, aspect ratio, and rigidity in addition to metal contamination. A number of current studies indicate that a potential key step in the initiation of inflammation leading to lung injury is activation of the NLRP3 inflammasome (Cassel et al., 2008; Dostert et al., 2008; Gasse et al., 2007). The NLRP3 inflammasome is present in macrophages, which would be one of the first cells to encounter any inhaled nanomaterial and therefore represents a logical target cell to consider. For in vitro assay purposes, the THP-1 monocytic-like cell has many advantages. It is a not a transformed cell, but can be differentiated by agents such asphorbol esters into macrophage-like cells in a reproducible manner for mechanistic and in vitro testing purposes.

In the current study we utilised the THP-1 cell model to evaluate the role that Ni in various formats in nanomaterials could have in contributing to causing cell toxicity and activating the NLRP3 inflammasome. Furthermore, this study evaluated the potential relationship between toxicity and NLRP3 inflammasome activation. The results suggested that Ni content present on MWCNT either as left over catalyst from the preparation of the nanomaterials or when added to the sidewalls of MWCNT was effective in stimulating the NLRP3 inflammasome in a Ni-content dependent manner. However, the Ni content did not correlate with cytotoxicity. Of the other common metal contaminants on MWCNT, no other metals correlated with NLRP3 activation, while cobalt and molybdenum on commercial MWCNT weakly correlated with cytotoxicity.

In contrast to a previous report (Caicedo et al., 2009) using a soluble form of Ni ($NiCl_2$) we did not observe any NLRP3 inflammasome activation or cytotoxicity using a similar model of THP-1 cells. The reason for the difference in outcome is not clear since similar dose ranges were tested in both studies. In addition, no significant biological activity for either cytotoxicity or NLRP3 inflammasome activation was detected in the current study using Ni nanopowder. One of the reasons for using these control materials was to determine whether the information would help to determine what was the biological active form of Ni causing both toxicity and NLRP3 inflammasome activation when present on MWCNT. As demonstrated in this study the presence of Ni either as left over catalyst or added to the sidewall of MWCNT was biologically active. Based on our current understanding of the mechanism of NLRP3 activation with other particulates [asbestos and silica (Dostert et al., 2008; Cassel et al., 2008)] as well as certain nanomaterials [TiO_2 nanobelts (Hamilton et al., 2009; Sager et al., 2012)] it appears that lysosomal rupture is required as an upstream signal for assembly of the NLRP3 inflammasome and caspase-1 activation. Mechanisms to explain lysosomal rupture are not well defined, but could be explained when particles too large to be contained within lysosomes are internalised (e.g., long aspect ratio particles such as TiO_2 nanobelts and asbestos fibres). This was well described in a study using rigid needle-like MWCNT to stimulate NLRP3 inflammasome in primed macrophages (Palomaki et al., 2011). Alternatively, particles that either directly cause the lysosomal member to degrade or stimulate excessive free radical production may provide another mechanism (Morishige et al., 2010). In fact, Ni is an effective metal catalyst for redox cycling (Pourahmad et al., 2003). Alternatively, Ni could participate in displacing proteins involved in lysosomal stability from the lysosome interior (e.g., LAMP proteins). This would provide an explanation why soluble Ni may not be very effective compared to Ni on particulates that would be effectively delivered to the interior of lysosomes. In addition, the NiO coating on the Ni nanopowder may prevent effective Ni bioactivity inside of lysosomes.

Although the mechanism to explain the apparent bioactivity of Ni within lysosomes is not yet clear, it was evident that the Ni in/on both forms on MWCNT used in this study was bioactive in stimulating NLRP3 inflammasome assembly leading to IL-1β release. Therefore, consistent with other recent studies (Liu et al., 2007, 2008) the presence of Ni on nanomaterials needs to be considered as contributing to potential human health effects. CNT have been shown to cause lung inflammation and formation of granuloma-like structures and lung fibrosis following instillation in rodent models (Mercer et al., 2010, 2011; Warheit et al., 2004; Lam et al., 2004). Consequently, the mechanism of the lung pathology from MWCNT exposure may well be linked to the activation of the NLRP3 inflammasome with IL-1β release. IL-1β has been shown to be

an important mediator of inflammation in many tissues including the lung (Dinarello, 2010, 2011b).

In contrast to the correlation between Ni content on MWCNT and NLRP3 inflammasome activation, there was not a similar correlation between Ni content and cytotoxicity. These findings would suggest that different mechanisms are involved in the two endpoints used in this study. Therefore, future studies with nanomaterials should consider multiple endpoints that include not only cytotoxicity, but also measurements of bioactivity that are consistent with known mechanisms of pathology in the relevant organ systems under investigation. Furthermore, the current study suggests that the THP-1 cell line could be used to rapidly screen for bioactivity of new nanomaterials.

Acknowledgements

This work was supported by NIH grants RC2-ES018742, P20-RR017670 and F32 ES019816.

References

Buford, M.C., Hamilton Jr., R.F. and Holian, A. (2007) 'A comparison of dispersing media for various engineered carbon nanoparticles', *Part Fibre Toxicol*, Vol. 4, 6p.

Caicedo, M., Desai, R., McAllister, K., Reddy, A., Jacobs, J.J. and Hallab, N.J. (2009) 'Soluble and particulate Co-Cr-Mo alloy implant metals activate the inflammasome danger signaling pathway in human macrophages: a novel mechanism for implant debris reactivity', *Journal of Orthopaedic Research*, Vol. 27, pp.847–854.

Cassel, S.L., Eisenbarth, S.C., Iyer, S.S., Sadler, J.J., Colegio, O.R., Tephly, L.A., Carter, A.B., Rothman, P.B., Flavell, R.A. and Sutterwala, F.S. (2008) 'The Nalp3 inflammasome is essential for the development of silicosis', *Proc. Natl. Acad. Sci.*, USA, Vol. 105, pp.9035–9040.

Chen, C.H., Su, H.C., Chuang, S.C., Yen, S.J., Chen, Y.C., Lee, Y.T., Chen, H., Yew, T.R., Chang, Y.C., Yeh, S.R. and Yao, D.J. (2010) 'Hydrophilic modification of neural microelectrode arrays based on multi-walled carbon nanotubes', *Nanotechnology*, Vol. 21, 485501p.

Cortijo, J., Milara, J., Mata, M., Donet, E., Gavara, N., Peel, S.E., Hall, I.P. and Morcillo, E.J. (2010) 'Nickel induces intracellular calcium mobilization and pathophysiological responses in human cultured airway epithelial cells', *Chemico-biological Interactions*, Vol. 183, pp.25–33.

Davis, B.K., Wen, H. and Ting, J.P. (2011) 'The inflammasome NLRs in immunity, inflammation, and associated diseases', *Annual Review of Immunology*, Vol. 29, pp.707–735.

Dinarello, C.A. (2009) 'Interleukin-1 beta and the autoinflammatory diseases', *The New England Journal of Medicine*, Vol. 360, pp.2467–2470.

Dinarello, C.A. (2010) 'Blocking interleukin-1 beta in acute and chronic autoinflammatory diseases', *J. Intern. Med.*, Vol. 269, pp.16–28.

Dinarello, C.A. (2011a) 'Interleukin-1 in the pathogenisis and treatment of inflamatory diseases', *Blood*, Vol. 117, pp.3720–3732.

Dinarello, C.A. (2011b) 'Interleukin-1 in the pathogenesis and treatment of inflammatory diseases', *Blood*, Vol. 117, pp.3720–3732.

Donaldson, K. and Stone, V. (2003) 'Current hypotheses on the mechanisms of toxicity of ultrafine particles', *Annali dell'Istituto superiore di sanita*, Vol. 39, pp.405–410.

Dostert, C., Petrilli, V., van Bruggen, R., Steele, C., Mossman, B.T. and Tschopp, J. (2008) 'Innate immune activation through Nalp3 inflammasome sensing of asbestos and silica', *Science*, Vol. 320, pp.674–677.

Gao, B., Yuan, C.Z., Su, L.H., Chen, L. and Zhang, X.G. (2008) 'Nickel oxide coated on ultrasonically pretreated carbon naontubes for supercapacitor', *Journal of Solid State Electrochemistry*, Vol. 13, pp.1251–1257.

Gasse, P., Mary, C., Guenon, I., Noulin, N., Charron, S., Schnyder-Candrian, S., Schnyder, B., Akira, S., Quesniaux, V.F., Lagente, V., Ryffel, B. and Couillin, I. (2007) 'IL-1R1/MyD88 signaling and the inflammasome are essential in pulmonary inflammation and fibrosis in mice', *J. Clin. Invest.*, Vol. 117, pp.3786–3799.

Hamilton, R.F., Wu, N., Porter, D., Buford, M., Wolfarth, M. and Holian, A. (2009) 'Particle length-dependent titanium dioxide nanomaterials toxicity and bioactivity', *Part Fibre Toxicol*., Vol. 6, 35p.

Harris, P. (1999) *Carbon Nanotubes and Related Structures: New Materials for the 21st Century*, Cambridge University Press, Cambridge.

Inoue, K., Koike, E., Yanagisawa, R., Hirano, S., Nishikawa, M. and Takano, H. (2009) 'Effects of multi-walled carbon nanotubes on a murine allergic airway inflammation model', *Toxicology and Applied Pharmacology*, Vol. 237, pp.306–316.

Lam, C.W., James, J.T., McCluskey, R. and Hunter, R.L. (2004) 'Pulmonary toxicity of single-wall carbon nanotubes in mice 7 and 90 days after intratracheal instillation', *Toxicological Sciences: An Official Journal of the Society of Toxicology*, Vol. 77, pp.126–134.

Lang, J.W., Kong, L.B., Wu, W.J., Luo, Y.C. and Kang, L. (2008) 'Facile approach to prepare loose-packed NiO nano-flakes materials for supercapacitors', *Chemical Communications*, Vol. 35, pp.4213–4215, Cambridge.

Lee, J.Y., Liang, K., An, H.K. and Lee, Y.H. (2005) 'Nickel oxide/carbon nanotubes nanocoposite for electrochemical capacitance', *Synthetic Metals*, Vol. 150, pp.153–157.

Lin, P., Qiujie, S., Hong, B., Xiaojing, L., Shi, Y., Shi, Z., Zheng, M. and Dong, Q. (2010) 'The nickel oxide/CNT composites with high capacitance for supercapacitor', *Journal of the Electrochemical Society*, Vol. 157, pp.A818–A823.

Liu, X., Guo, L., Morris, D., Kane, A.B. and Hurt, R.H. (2008) 'Targeted removal of bioavailable metal as a detoxification strategy for carbon nanotubes', *Carbon*, Vol. 46, pp.489–500.

Liu, X.Y., Gurel, V., Morris, D., Murray, D.W., Zhitkovich, A., Kane, A.B. and Hurt, R.H. (2007) 'Bioavailability of nickel in single-wall carbon nanotubes', *Advanced Materials*, Vol. 19, pp.2790–2796.

Madl, A.K. and Pinkerton, K.E. (2009) 'Health effects of inhaled engineered and incidental nanoparticles', *Critical Reviews in Toxicology*, Vol. 39, pp.629–658.

Mercer, R.R., Hubbs, A.F., Scabilloni, J.F., Wang, L., Battelli, L.A., Friend, S., Castranova, V. and Porter, D.W. (2011) 'Pulmonary fibrotic response to aspiration of multi-walled carbon nanotubes', *Part Fibre Toxicol*., Vol. 8, 21p.

Mercer, R.R., Hubbs, A.F., Scabilloni, J.F., Wang, L., Battelli, L.A., Schwegler-Berry, D., Castranova, V. and Porter, D.W. (2010) 'Distribution and persistence of pleural penetrations by multi-walled carbon nanotubes', *Part Fibre Toxicol*., Vol. 7, 28p.

Morishige, T., Yoshioka, Y., Inakura, H., Tanabe, A., Yao, X., Narimatsu, S., Monobe, Y., Imazawa, T., Tsunoda, S., Tsutsumi, Y., Mukai, Y., Okada, N. and Nakagawa, S. (2010) 'The effect of surface modification of amorphous silica particles on NLRP3 inflammasome mediated IL-1beta production, ROS production and endosomal rupture', *Biomaterials*, Vol. 31, pp.6833–6842.

Nam, S.H., Kim, Y.S., Shim, H.S., Choi, S.M., Kim, H.J. and Kim, W.B. (2008) 'Size controlled nickel oxide nanoparticles on carbon nanotubes for supercapacitor electrode', *Journal of Nanoscience and Nanotechnology*, Vol. 8, pp.5427–5432.

Oberdorster, G. (2010) 'Safety assessment for nanotechnology and nanomedicine: concepts of nanotoxicology', *Journal of Internal Medicine*, Vol. 267, pp.89–105.

Palomaki, J., Valimaki, E., Sund, J., Vippola, M., Clausen, P.A., Jensen, K.A., Savolainen, K., Matikainen, S. and Alenius, H. (2011) 'Long, needle-like carbon nanotubes and asbestos activate the NLRP3 inflamma some through a similar mechanism', *ACS Nano*, Vol. 5, pp.6861–6870.

Pourahmad, J., O'Brien, P.J., Jokar, F. and Daraei, B. (2003) 'Carcinogenic metal induced sites of reactive oxygen species formation in hepatocytes', *Toxicol in Vitro*, Vol. 17, pp.803–810.

Rocha, M.A. (2009) 'Preparation and characterization of colloidal Ni(OH)2/bentonite composites', *Materials Research Bulletin*, Vol. 44, pp.970–976.

Rock, K.L., Latz, E., Ontiveros, F. and Kono, H. (2010) 'The sterile inflammatory response', *Annual Review of Immunology*, Vol. 28, pp.321–342.

Sager, T.M., Wolfarth, M.W., Andrew, M., Hubbs A., Chen, T., Porter, D.W., Wu, N., Yang, F., Hamilton Jr., R.F. and Holian, A. (2012) 'Analysis of the effect of multi-walled carbon nanotube surface modification on bioactivity and inflammasome activation', Submitted to *Journal Nanotoxicol*.

Tschopp, J. and Schroder, K. (2010) 'NLRP3 inflammasome activation: the convergence of multiple signalling pathways on ROS production?', *Nat. Rev. Immunol.*, Vol. 10, pp.210–215.

Warheit, D.B., Laurence, B.R., Reed, K.L., Roach, D.H., Reynolds, G.A. and Webb, T.R. (2004) 'Comparative pulmonary toxicity assessment of single-wall carbon nanotubes in rats', *Toxicol. Sci*., Vol. 77, pp.117–125.

Yazdi, A.S., Guarda, G., Riteau, N., Drexler, S.K., Tardivel, A., Couillin, I. and Tschopp, J. (2010) 'Nanoparticles activate the NLR pyrin domain containing 3 (Nlrp3) inflammasome and cause pulmonary inflammation through release of IL-1 alpha and IL-1 beta', *Proc. Natl. Acad. Sci.*, USA, Vol. 107, pp.19449–19454.

Supplemental figures

Figure 1 TEM image of the Ni nanoparticles, (a) low-magnification, (b) high-resolution image showing the lattice fringe of Ni(111) (see online version for colours)

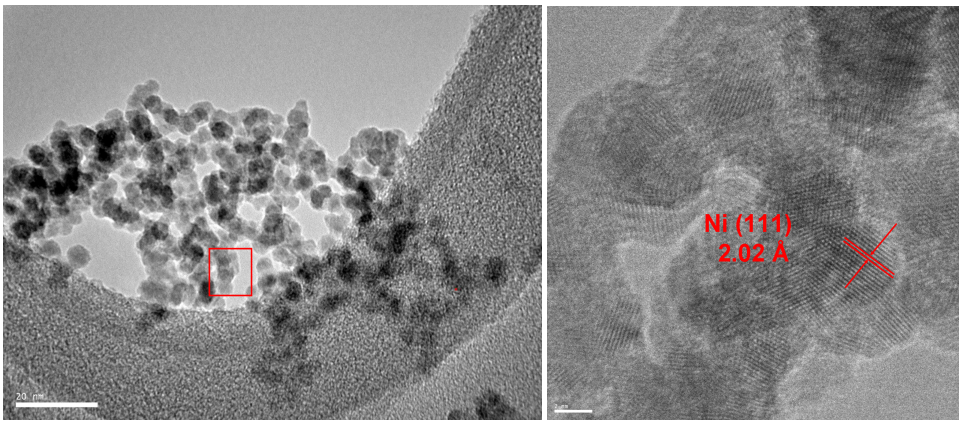

(a) (b)

Note: Figure 1(b) was taken from the square labelled in Figure 1(a).

Figure 2 SEM image of Ni-decorated MWCNTs with a high level of Ni

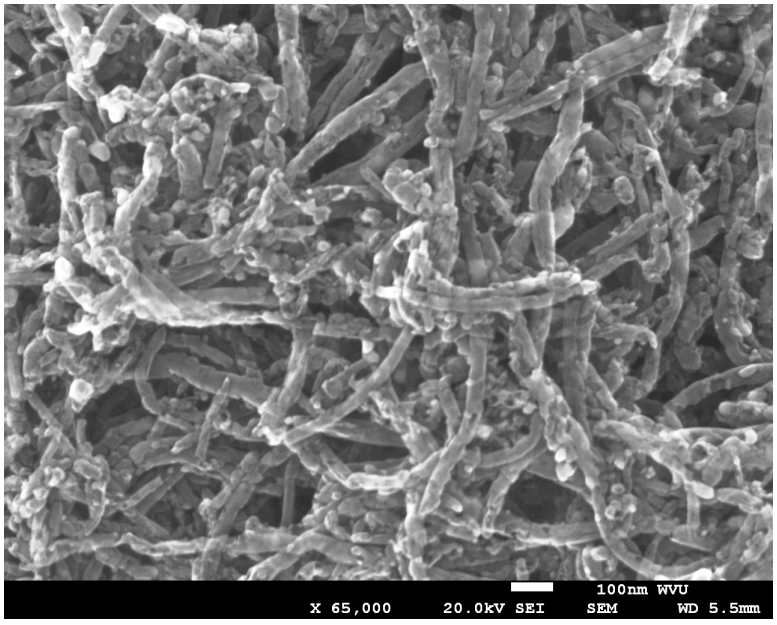

Figure 3 Raw data for scatterplots found in Figures 1 and 2, (a) Toxicity data by MTS assay for 24 MWCNT cultured with THP-1 cells for 24 hours at 25 µg/ml (data arranged from lowest Ni to highest Ni from left to right) (b) IL-1β release data for 24 MWCNT cultured with THP-1 cells for 24 hours at 25 µg/ml (data arranged from lowest Ni to highest Ni from left to right)

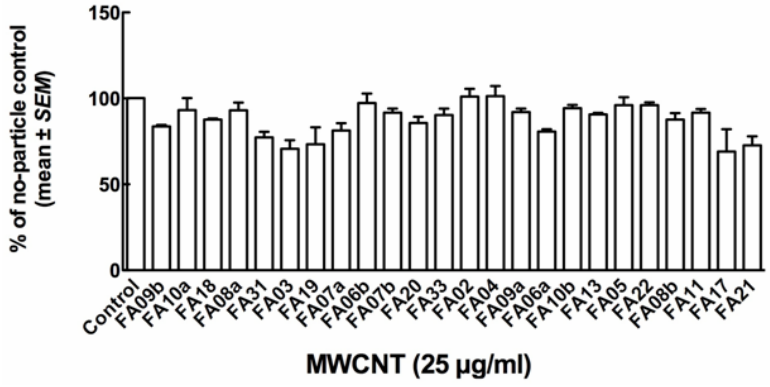

(a)

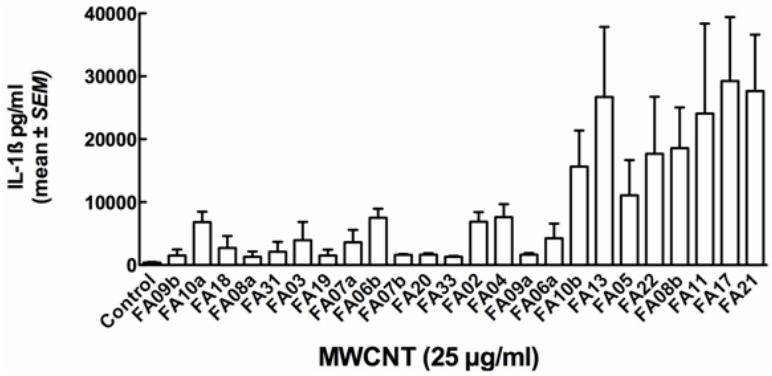

(b)